Fast Exponentially Convergent Solution of Electromagnetic Scattering From Multilayer Concentric Magnetodielectric Cylinders by the Spectral Integral Method

Zhen Guan, Yuxian Zhang, *Member, IEEE*, Feng Han, *Member, IEEE*, Chunhui Zhu, and Qing Huo Liu, *Fellow, IEEE*

***Abstract*— The multilayer surface integral equations (SIEs) for electromagnetic scattering by infinitely long magnetodielectric cylinders with an arbitrary number of layers are derived and solved by the spectral integral method (SIM). Singularity subtraction for the 2-D Green's function is used to enhance the computation accuracy and achieve exponential convergence. The final matrix equation after discretization is formed in the Fourier spectral domain rather than the spatial domain, which greatly expedites the SIM solution by accelerating the convolution via the fast fourier transform (FFT) algorithm. A recursive method is proposed to solve the spectral integral equations instead of using an iterative method to lower the computation complexity. Numerical examples for ordinary multilayer cylinders and invisibility cloak cylinders are presented to validate the SIM results by comparing the total fields, scattered fields, and radar cross section (RCS) to analytical solutions or finite-element simulations. They verify that the recursive solution has a complexity of $O(MN \log N)$ for an M-layer cylinder with N discrete points on each interface. Meanwhile, the SIM outperforms the analytical method because only the 0th-order and 1st-order special functions (Bessel functions and Hankel functions) are used in the SIM but higher-order functions are necessary for the analytical method to maintain the accuracy.**

***Index Terms*— Layered invisibility cloak, multilayer cylinder scattering, recursive solution, spectral integral method (SIM), surface integral equations (SIEs).**

I. Introduction

In the past three decades, the electromagnetic (EM) scattering by cylinders has been widely studied. The research is not only for academic purpose but also well applied in microwave engineering such as the design of superstrate-loaded conformal microstrip antennas [1] and investigation of the absorption characteristics of EM radiation for multilayered cylindrical models of human torsos [2]. Both analytical and numerical solutions have been developed for the EM scattering by multilayer cylinders.

The most straightforward analytical solution for EM scattering by dielectric or perfect electric conductor (PEC) cylinders is obtained by expanding the wavefield in terms of cylindrical eigenfunctions, i.e., Bessel and Hankel functions of various orders, and solving the expansion coefficients by matching the boundary conditions [3]. Another popular analytical method is to expand the wavefield or Green's function by the vector wave functions [4]. This has been successfully used to solve the EM scattering by multilayer chiral cylinders [5] and elliptical cylinders [6]. However, analytical methods suffer from the extreme arguments or high orders and the convergence problem when cylindrical functions are evaluated for electrically large objects. Therefore, a pseudoanalytical method is proposed to overcome these problems by using different sets of range-conditioned, modified cylindrical functions [7].

Besides the aforementioned analytical solutions, numerical computation is another important method to solve EM scattering by cylinders. The easiest way is to formulate the EM scattering by cylinders via integral equations and solve them by the method of moments (MoMs) [8], [9] which can be further accelerated by the spectral integral method (SIM) [10], [11]. The SIM is efficient to compute EM scattering with a low spatial sampling density (SD) for dielectric and PEC objects with closed boundaries buried in a homogeneous background or a layered medium [12], smooth multilayered bodies of revolution (BoRs) [13], and a lossy circularly layered dielectric cylinder illuminated by a beam field [14]. Other techniques such as the method of auxiliary sources (MASs) developed by Zaridze *et al.* [15] have been successfully applied to scattering problems for dielectric circular cylinders and have been extended to layered dielectric cylinders by Tsitsas *et al.* [16].

The surface integral equation (SIE) is a numerical method commonly used to solve PEC [17] or dielectric cylinder scattering [18] problems. The importance of SIE in the

Manuscript received August 6, 2019; revised December 7, 2019 and January 13, 2020; accepted January 26, 2020. Date of publication March 2, 2020; date of current version June 3, 2020. This work was supported by the National Key R&D Program of the Ministry of Science and Technology of China under Grant 2018YFC0603503 and Grant 2018YFF01013300. *(Corresponding authors: Feng Han; Qing Huo Liu.)*

Zhen Guan is with the School of Mathematical Sciences, Institute of Electromagnetics and Acoustics, Xiamen University, Xiamen 361005, China.

Yuxian Zhang is with the Institute of Microscale Optoelectronics, Shenzhen University, Shenzhen 518060, China.

Feng Han and Chunhui Zhu are with the Fujian Provincial Key Laboratory of Electromagnetic Wave Science and Detection Technology, Institute of Electromagnetics and Acoustics, Xiamen University, Xiamen 361005, China (e-mail: feng.han@xmu.edu.cn).

Qing Huo Liu is with the Department of Electrical and Computer Engineering, Duke University, Durham, NC 27708 USA (e-mail: qhliu@duke.edu).

Color versions of one or more of the figures in this article are available online at http://ieeexplore.ieee.org.

Digital Object Identifier 10.1109/TMTT.2020.2973632

solution, both theoretical and practical, of certain types of boundary value problems (BVPs) is universally recognized since 1960s. The equivalence of the SIE and initial BVP and the uniqueness and existence of the solution to the SIE with radiation boundary condition were demonstrated by Leis [19]. Then the application of SIE to BVP for Laplace's equation and for the Helmholtz equation is discussed by Burton and Miller [20]. Rao *et al.* [21] and Chew [22] developed this theory more widely for EM scattering, and Hu [23], [24] and Zaman [25] applied it to acoustic wave scattering. In acoustics, Schuster [26] adopted the SIE method to solve the line source response of concentric cylinders filled with acoustic materials. Zhu *et al.* [18] solve EM and acoustic scattering by penetrable cylinders based on [26] but using the SIM. However, this article was for a single cylinder and the permeability was assumed constant.

In this article, we extend our previous direct SIM [18] to arbitrary multilayer cylinders. Meanwhile, the magnetic property variation of the layered scatterers is considered, i.e., the layered cylinders can be arbitrary magnetodielectric media. Therefore, SIEs are formulated for EM scattering by multilayer concentric magnetodielectric cylinders. The SIM proposed in [10] is used to solve the SIEs in the spectral domain. The singularity in the 2-D Green's function is handled by a truncated Fourier series. In addition, a fast recursive algorithm based on the boundary continuity of tangential electric and magnetic fields is proposed to solve the SIEs. It is demonstrated that as a direct (noniterative) method, the SIM can provide an exponentially accurate result and guarantee a less than 0.1‰ error with an SD of only three points per wavelength (PPW). Four numerical examples with 4 layers and 20 layers are presented to validate the applicability of the proposed SIM for arbitrary number of layers, thickness, and electrical sizes. Meanwhile, the computation accuracy with and without the singularity subtraction of Green's functions is compared. The effects of the SD (in terms of PPW values) on the SIM solutions are shown to verify the rapid convergence of the SIM. Furthermore, the SIM is used to solve the wavefield for a layered invisibility cloak and the scattering width (SW) with or without the cloak is compared. Finally, the computation parameters are listed for arbitrary multilayer magnetodielectric cylinders.

This article is organized as follows. In Section II, the SIEs are derived for multilayer magnetodielectric cylinders, and the singularity subtraction of Green's functions is discussed. The SIEs are discretized and the matrix equations are formulated in the Fourier spectral domain. The SIM is applied to SIEs to obtain recursive solutions. In Section III, numerical examples are given to validate our method. Conclusions and discussions are presented in Section IV.

II. SIE Formulation for Multilayer Concentric Magnetodielectric Cylinders

In this section, we will derive the SIEs for EM scattering from multilayer magnetodielectric cylinders. The number of layers is arbitrary, and both the permittivity and permeability in different layers can be different. In this article, we consider the transverse magnetic (TM) wave, i.e., TM-polarized incident EM wave. The transverse electric (TE) polarization solution can be obtained by duality.

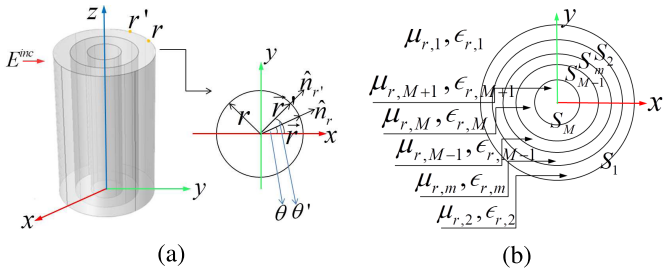

Fig. 1. (a) Infinitely long multilayer magnetodielectric concentric cylinder placed along the z-axis, with the incident plane wave $\mathbf{E^{inc}}$ propagating parallel to the cross section plane (xy) of the cylinder. (b) xy plane sectional view of the multilayer cylinder.

Consider an infinitely long multilayer magnetodielectric concentric cylinder with the axis parallel to the z direction in the Cartesian coordinate system, as shown in Fig. 1(a). The incident plane wave is $\hat{z}$ polarized. As shown in [3], if the wave is propagating in the x direction, the incident wave field $\mathbf{E^{inc}}$ can be expanded as

$$\begin{aligned}\mathbf{E^{inc}} &= \hat{z}e^{-jk_1x} = \hat{z}e^{-jk_1r\cos\theta} \\ &= \hat{z}\sum_{n=-\infty}^{n=\infty} j^{-n}J_n(k_1r)e^{jn\theta} \end{aligned} \tag{1}$$

where J_n is the first kind Bessel function, and k_1 is the wavenumber of the background medium in which the cylinder is located.

A. Formulation of SIEs

For clarity, the xy plane sectional view of the magnetodielectric concentric cylinder is illustrated in Fig. 1(b). The cylinder is composed of different EM materials. The relative permeability and permittivity are $(\mu_{r,1}, \epsilon_{r,1}), \ldots, (\mu_{r,M+1}, \epsilon_{r,M+1})$ from outside to inside. The radius of each layer from outside to inside is $r_m (1 \leqslant m \leqslant M)$, and the corresponding wavenumber of each layer is $k_m = k_0(\mu_{r,m}\epsilon_{r,m})^{1/2}$, where k_0 is the wavenumber in free space. $S_m (1 \leqslant m \leqslant M)$ is the interface between layers m and $m+1$.

According to the Stratton-Chu formula [27], the scattered electric field can be written as

$$\begin{aligned}&\mathbf{E^{sct}} \\ &= \oint\{j\omega\mu[\hat{n}'\times\mathbf{H}(t')]g(\mathbf{r},\mathbf{r}')+[\hat{n}'\times\mathbf{E}(t')]\times\nabla' g(\mathbf{r},\mathbf{r}')\}dt' \\ &= \mu_r\oint jk_0\tilde{\mathbf{J}}(t')g(\mathbf{r},\mathbf{r}')dt' - \hat{n}'\times\oint\frac{\partial g(\mathbf{r},\mathbf{r}')}{\partial n'}\hat{t}(t')E_z(t')dt' \\ &= \hat{z}\oint[\mu_r jk_0 g(\mathbf{r},\mathbf{r}')\tilde{J}_z(t') - \frac{\partial g(\mathbf{r},\mathbf{r}')}{\partial n'}E_z(t')]dt' \end{aligned} \tag{2}$$

where the unknown current density has been parameterized with the arc length t in the tangential $\hat{t}$ direction, $\tilde{\mathbf{J}} = \eta_0\hat{n}\times\mathbf{H} = \hat{z}\eta_0 H_t = \hat{z}\tilde{J}_z$ on the surface S radiating in the background medium are used to produce the scattered fields inside the object, $\hat{n}$ is the outward normal direction, and $g(\mathbf{r},\mathbf{r}')$ is the 2-D scalar Green's function.

In virtue of (2) and the surface equivalent principle [3], we can obtain the multilayer SIEs in which there are totally M sets of equations as (3), as shown at the bottom of this page, with $1 \leqslant m \leqslant M$. I is the identity operator, and the specific expressions of the operators L, K are as follows [28]:

$$L_\tau[\tilde{J}_{s,m}] = -jk_0 \int_{S_m} g_\tau(\mathbf{r}, \mathbf{r}') \tilde{J}_{z,m}(t') dt', \quad \tau = m, m+1 \tag{4a}$$

$$K_\tau[E_{z,m}] = \int\!\!\!\!\!\!- _{S_m} \frac{\partial g_\tau(\mathbf{r}, \mathbf{r}')}{\partial n'} E_{z,m}(t') dt', \quad \tau = m, m+1 \tag{4b}$$

where $\int\!\!\!\!\!\!-$ denotes the Cauchy principal-value integral. One should note that S_0 and S_{M+1} do not exist, and thus, the corresponding terms in (3) have no contribution to the multilayer SIEs. g_m is the 2-D scalar Green's function in the mth layer, which corresponds to the solution of the following Helmholtz equation:

$$\nabla^2 g_m + k^2 g_m = -\delta(\mathbf{r} - \mathbf{r}') \tag{5}$$

subject to the Sommerfeld radiation boundary condition. In Green's function g_m is expressed as

$$\begin{aligned} g_m &= g_m(k_m R_{pq}) \\ &= g_m\big(k_m|\mathbf{r}_p - \mathbf{r}'_q|\big) = -\frac{j}{4} H_0^{(2)}\big(k_m|\mathbf{r}_p - \mathbf{r}'_q|\big) \end{aligned} \tag{6}$$

where $\mathbf{r}_p$ is the field point locating on the pth interface, and $\mathbf{r}'_q$ is the equivalent source point locating on the qth interface. R_{pq} is the distance between $\mathbf{r}_p$ and $\mathbf{r}'_q$. $H_0^{(2)}$ is the 0th-order Hankel function of the second kind. If we represent $\mathbf{r}_p$ in the Cartesian system with (x_p, y_p) and $\mathbf{r}'_q$ with (x'_q, y'_q), we have $x_p = r_p \cos\theta$, $y_p = r_p \sin\theta$, $x'_q = r_q \cos\theta'$, and $y'_q = r_q \sin\theta'$, where $1 \leqslant p, q \leqslant M$ and $\theta, \theta' \in [0, 2\pi)$, as shown in Fig. 1(a). r_p and r_q are the radius of the pth and the qth interface, respectively.

By following the above definitions, we can easily obtain:

$$R_{pq} = \begin{cases} 2r_p \left|\sin\left(\frac{\theta - \theta'}{2}\right)\right|, & p = q \\ \sqrt{r_p^2 + r_q^2 - 2r_p r_q \cos(\theta - \theta')}, & |p - q| = 1. \end{cases} \tag{7}$$

Hence, g_m in (6) can be readily evaluated.

The normal derivative of Green's function in the cylindrical coordinate system is

$$\frac{\partial g_m}{\partial n'}(\mathbf{r}_p, \mathbf{r}'_q) = \frac{jk_m}{4} H_1^{(2)}(k_m R_{pq}) \cdot \frac{\mathbf{R}_{pq} \cdot \hat{n}'}{R_{pq}} \tag{8}$$

where

$$\frac{\mathbf{R}_{pq} \cdot \hat{n}'}{R_{pq}} = \begin{cases} \left|\sin\left(\frac{\theta - \theta'}{2}\right)\right|, & p = q \\ \frac{R_{pq}^2 + r_q^2 - r_p^2}{2R_{pq} r_q}, & p \neq q \end{cases} \tag{9}$$

and $H_1^{(2)}$ is the first-order Hankel function of the second kind.

B. Singularity Subtraction

In the SIEs (3), when the field point $\mathbf{r}_p$ and equivalent source point $\mathbf{r}'_q$ overlap, both g_m and $\partial g_m / \partial n$ will show singularities.

When $p = q$, we have $\xi \equiv k_m R_{pq} = 2r_p k_m |\sin\frac{\delta\theta}{2}|$ where $\delta\theta = \theta - \theta'$, then we separate integral kernels in (4) into their smooth parts and singular parts as [18], [24]

$$H_0^{(2)}(\xi) = \bar{H}_0^{(2)}(\xi) - \frac{2j}{\pi} J_0(\xi) \ln|2\sin\frac{\delta\theta}{2}| \tag{10a}$$

$$\begin{aligned} \frac{\partial g_m}{\partial n'} &= [J_1(\xi) - jY_1(\xi)] \frac{jk_m \hat{n}' \cdot \mathbf{R}_{pq}}{4R_{pq}} \\ &= \left[\frac{-1}{\xi} + \ln\left|\frac{\xi}{2}\right| J_1(\xi) + \sum_{s=0}^{\infty} a_{2s+1} \xi^{2s+1}\right] \\ &\quad \times \frac{-k_m}{2\pi}\left|\sin\frac{\delta\theta}{2}\right| \\ &= \bar{g}'_m(\xi) + \ln\left|2\sin\frac{\delta\theta}{2}\right| J_1(\xi) \frac{k_m}{2\pi}\left|\sin\frac{\delta\theta}{2}\right| \end{aligned} \tag{10b}$$

Note that at $\theta = \theta'$, the second term in the right side of (10a) is singular, while that in (10b) is finite but has a derivative discontinuity because of the presence of $|\sin\frac{\delta\theta}{2}|$.

We expand $\ln|2\sin(\frac{\theta - \theta'}{2})|$ by Fourier series [23], [24]

$$\ln\left|2\sin\frac{\theta - \theta'}{2}\right| = -\sum_{n=1}^{\infty} \frac{\cos n(\theta - \theta')}{n} = \sum_{n=-\infty}^{+\infty} a_n e^{jn(\theta - \theta')} \tag{11}$$

in which $a_0 = 0$ and $a_n = -1/(2|n|)$ for $n \neq 0$. We empirically truncate enough terms to $2N$ terms for $\ln|2\sin(\frac{\theta - \theta'}{2})|$ to evaluate the singularity analytically as in [18].

C. Discretization

Before SIEs are solved, discretization is needed. By referring to the details in [24], we discretize all interface layers synchronously. We divide the whole circumference into N equal arc elements as $\theta_n = \Delta\theta(n-1)$, where $n \in [1, N]$

$$\begin{bmatrix} 0 & 0 & \mu_{r,m} L_m & K_m - \frac{1}{2} I & -\mu_{r,m} L_m & -K_m \\ \mu_{r,m+1} L_{m+1} & K_{m+1} & -\mu_{r,m+1} L_{m+1} & -K_{m+1} - \frac{1}{2} I & 0 & 0 \end{bmatrix} \begin{bmatrix} \tilde{J}_{s,m+1} \\ E_{z,m+1} \\ \tilde{J}_{s,m} \\ E_{z,m} \\ \tilde{J}_{s,m-1} \\ E_{z,m-1} \end{bmatrix} = \begin{bmatrix} -E_m^{inc} \\ E_{m+1}^{inc} \end{bmatrix} \tag{3}$$

and $\Delta\theta = (2\pi/N)$. Then, when $\mathbf{r} \in S_m$, the SIEs in (3) can be compactly rewritten as

$$\begin{cases} -T_{m,m}(\theta_n) + T_{m,m-1}(\theta_n) \\ = \dfrac{E_{z,m}(\theta_n)}{2} - E^{inc}_{z,m}(\theta_n) \\ -T_{m+1,m+1}(\theta_n) + T_{m+1,m}(\theta_n) \\ = \dfrac{E_{z,m}(\theta_n)}{2} + E^{inc}_{z,m+1}(\theta_n) \end{cases} \tag{12}$$

for $n = 1, \ldots, N$, where

$$T_{m,q}(\theta_n) = \sum_{n'=1}^{N} \iota_m\big(R_{pq}, \theta_n, \theta'_{n'}\big)\tilde{J}_{z,q}\big(\theta'_{n'}\big) - \sum_{n'=1}^{N} \kappa_m\big(R_{pq}, \theta_n, \theta'_{n'}\big)E_{z,q}\big(\theta'_{n'}\big) \tag{13a}$$

$$\iota_m\big(R_{pq}, \theta_n, \theta'_{n'}\big) = \mu_{r,m} jk_0 r_q \Delta\theta g_m\big(k_m R_{pq}\big(\theta_n, \theta'_{n'}\big)\big) \tag{13b}$$

$$\kappa_m\big(R_{pq}, \theta_n, \theta'_{n'}\big) = r_q \Delta\theta \frac{\partial g_m\big(k_m R_{pq}\big(\theta_n, \theta'_{n'}\big)\big)}{\partial n'} \tag{13c}$$

where $1 \leqslant m \leqslant M+1$ is the mth layer, the subscript p is the field interface index, and subscript q refers to the qth interface in which the equivalent source points are located.

Equation (12) consists of $2NM$ coupled equations. The brute-force MoM solution of (12) is expensive with $O(M^3N^3)$ CPU time and $O(M^2N^2)$ memory. An iterative solution by using the biconjugate-gradient (BCG) method [12] can reduce the CPU time to $O(KM^2N^2)$, where K is the number of iterations. Here, we seek a direct solution with higher efficiency.

D. Fast Direct SIM With Recursive Solutions

In this article, we propose a recursive algorithm to solve the discretized SIEs to outperform even the iterative solution. Note that the interactions between the Green's function g_m or its normal derivative and E_z as well as $\tilde{J}_z$ in (13) are convolutions. Fast fourier transform (FFT) can be used to accelerate such convolutions. Therefore, we denote the Fourier transform of $\mu_{r,m} jk_0 r_q \Delta\theta g_m$, $\tilde{J}_{z,q}$, $r_q \Delta\theta(\partial g_m/\partial n) - 1/2$, $E_{z,q}$, and $E^{\text{inc}}_{z,q}$ as $\mathcal{L}^m_{p,q}$, $\mathcal{J}_{z,q}$, $\mathcal{K}^m_{p,q}$, $\mathcal{E}_{z,q}$, and $\mathcal{E}^{\text{inc}}_{z,q}$, respectively, where $\mathcal{L}^m_{p,q}$, $\mathcal{K}^m_{p,q}$ are the Fourier transform values in the mth layer. In this way, (12) is converted to N independent matrix equations which are completely uncoupled in the Fourier domain. The impedance matrix in each equation has the dimensions of $2M \times 2M$. These equations in the spectral domain are

$$\begin{cases} -\mathcal{L}^m_{m-1,m}\mathcal{J}_{z,m} + [\mathcal{K}^m_{m-1,m} + \frac{1}{2}]\mathcal{E}_{z,m} + \mathcal{L}^m_{m-1,m-1}\mathcal{J}_{z,m-1} \\ \quad - [\mathcal{K}^m_{m-1,m-1} + \frac{1}{2}]\mathcal{E}_{z,m-1} = \frac{\mathcal{E}_{z,m}}{2} - \mathcal{E}^{inc}_{z,m} \\ -\mathcal{L}^{m+1}_{m+1,m+1}\mathcal{J}_{z,m+1} + [\mathcal{K}^{m+1}_{m+1,m+1} + \frac{1}{2}]\mathcal{E}_{z,m+1} \\ \quad + \mathcal{L}^{m+1}_{m+1,m}\mathcal{J}_{z,m} - [\mathcal{K}^{m+1}_{m+1,m} + \frac{1}{2}]\mathcal{E}_{z,m} = \frac{\mathcal{E}_{z,m}}{2} - \mathcal{E}^{inc}_{z,m+1} \end{cases} \tag{14}$$

where all $\mathcal{J}_z$ terms are put in the left sides of the equations. The first one ($m = 1$) and the last one ($m = M$) are two single equations, and there are totally $M - 1$ pairs like

$$\mathcal{J}_{z,1} = \frac{(\mathcal{K}^1_{1,1} + 1/2)\mathcal{E}_{z,1} + \mathcal{E}^{inc}_{z,1}}{\mathcal{L}^1_{1,1}} \tag{15a}$$

$$\begin{cases} \mathcal{J}_{z,\alpha} = \frac{\Gamma^{(1)}_{\alpha,\beta}\mathcal{E}_{z,\beta} + \Gamma^{(1)}_{\beta,\beta}\mathcal{E}_{z,\alpha} + (\mathcal{L}^\beta_{\alpha,\beta} - \mathcal{L}^\beta_{\beta,\beta})\mathcal{E}^{inc}_{z,\beta}}{\Gamma^\beta} \\ \mathcal{J}_{z,\beta} = \frac{\Gamma^{(2)}_{\alpha,\alpha}\mathcal{E}_{z,\beta} + \Gamma^{(2)}_{\beta,\alpha}\mathcal{E}_{z,\alpha} + (\mathcal{L}^\beta_{\alpha,\alpha} - \mathcal{L}^\beta_{\beta,\alpha})\mathcal{E}^{inc}_{z,\beta}}{\Gamma^\beta} \end{cases} \tag{15b}$$

$$\mathcal{J}_{z,M} = \frac{(\mathcal{K}^{M+1}_{M,M} + 1/2)\mathcal{E}_{z,M} - \mathcal{E}^{inc}_{z,M+1}}{\mathcal{L}^{M+1}_{M,M}} \tag{15c}$$

where $1 \leqslant \alpha < M, \beta = \alpha + 1$ are positive integers. The expressions of $\Gamma^{(1)}_{\alpha,\alpha}$, $\Gamma^{(1)}_{\alpha,\beta}$, $\Gamma^{(2)}_{\beta,\alpha}$, $\Gamma^{(2)}_{\beta,\beta}$, Γ^β are given as

$$\Gamma^{(1)}_{\alpha,\beta} = \mathcal{L}^\beta_{\alpha,\beta}(\mathcal{K}^\beta_{\beta,\beta} + 1/2) - \mathcal{L}^\beta_{\beta,\beta}\mathcal{K}^\beta_{\alpha,\beta} \tag{16a}$$

$$\Gamma^{(1)}_{\beta,\beta} = \mathcal{L}^\beta_{\beta,\beta}(\mathcal{K}^\beta_{\alpha,\alpha} + 1/2) - \mathcal{L}^\beta_{\alpha,\beta}(\mathcal{K}^\beta_{\beta,\alpha} + 1) \tag{16b}$$

$$\Gamma^{(2)}_{\alpha,\alpha} = \mathcal{L}^\beta_{\alpha,\alpha}(\mathcal{K}^\beta_{\beta,\beta} + 1/2) - \mathcal{L}^\beta_{\beta,\alpha}\mathcal{K}^\beta_{\alpha,\beta} \tag{16c}$$

$$\Gamma^{(2)}_{\beta,\alpha} = \mathcal{L}^\beta_{\beta,\alpha}(\mathcal{K}^\beta_{\alpha,\alpha} + 1/2) - \mathcal{L}^\beta_{\alpha,\alpha}(\mathcal{K}^\beta_{\beta,\alpha} + 1) \tag{16d}$$

$$\Gamma^\beta = \mathcal{L}^\beta_{\alpha,\alpha}\mathcal{L}^\beta_{\beta,\beta} - \mathcal{L}^\beta_{\alpha,\beta}\mathcal{L}^\beta_{\beta,\alpha} \tag{16e}$$

In particular, when $\alpha = M$ or $\Gamma^{M+1} = \mathcal{L}^{M+1}_{M,M}$.

We then eliminate $\mathcal{J}_{z,1}$ in the first and the second equations in (15) and obtain the first relationship z_1 between $\mathcal{E}_{z,1}$ and $\mathcal{E}_{z,2}$ in (17). We repeat this process, e.g., eliminate $\mathcal{J}_{z,2}$ in the third and the fourth equations in (15) and obtain the second relationship z_2 for $\mathcal{E}_{z,1}$, $\mathcal{E}_{z,2}$ and $\mathcal{E}_{z,3}$. Totally, we can acquire M sets of equations

$$z_\gamma(\mathcal{E}_{z,\gamma-1}, \mathcal{E}_{z,\gamma}, \mathcal{E}_{z,\gamma+1}) \equiv a_\gamma \mathcal{E}_{z,\gamma-1} + b_\gamma \mathcal{E}_{z,\gamma} + c_\gamma \mathcal{E}_{z,\gamma+1} - d_\gamma = 0, \quad \gamma = 1, \cdots, M \tag{17}$$

where $a_1 = 0$ and $c_M = 0$. The other a_γ , b_γ, c_γ and d_γ are given below

$$a_\gamma = \Gamma^{\gamma+1}\Gamma^{(2)}_{\gamma,\gamma-1} \tag{18a}$$

$$b_\gamma = \Gamma^{\gamma+1}\Gamma^{(2)}_{\gamma-1,\gamma-1} - \Gamma^\gamma\Gamma^{(1)}_{\gamma+1,\gamma+1} \tag{18b}$$

$$c_\gamma = -\Gamma^\gamma\Gamma^{(1)}_{\gamma,\gamma+1} \tag{18c}$$

$$d_\gamma = \Gamma^\gamma(\mathcal{L}^{\gamma+1}_{\gamma,\gamma+1} - \mathcal{L}^{\gamma+1}_{\gamma+1,\gamma+1})\mathcal{E}^{inc}_{z,\gamma+1} - \Gamma^{\gamma+1}(\mathcal{L}^\gamma_{\gamma-1,\gamma-1} - \mathcal{L}^\gamma_{\gamma,\gamma-1})\mathcal{E}^{inc}_{z,\gamma} \tag{18d}$$

By substituting z_1 into z_2, we obtain the relationship between $\mathcal{E}_{z,2}$ and $\mathcal{E}_{z,3}$ as $y_2(\mathcal{E}_{z,2}, \mathcal{E}_{z,3}) = 0$, and by substituting y_2 into z_3, we obtain the relationship between $\mathcal{E}_{z,3}$ and $\mathcal{E}_{z,4}$ as $y_3(\mathcal{E}_{z,3}, \mathcal{E}_{z,4}) = 0$. In the same way, we can substitute z_M into z_{M-1} and obtain $y_{M-1}(\mathcal{E}_{z,M-2}, \mathcal{E}_{z,M-1}) = 0$. This process begins at the two sides of the equation system (17) and finally comes to only one equation and one unknown. When the final single equation is solved, other unknowns can be acquired recursively. Also, the mathematical derivations for such a recursive process are shown in Appendix A. This recursive algorithm is a direct noniterative solution and has computation cost as $O(NM)$ in total, which is obviously lower than the BCG method with the complexity of $O(NK(2M)^2)$ where K is the iteration number. After the unknown vector is solved, the inverse FFT with computational complexity of $O(N \log N)$ is applied to compute $\mathcal{E}_z$ in all interface layers. Thus, the computation complexity is $O(MN \log N)$ for the CPU time and $O(MN)$ for the memory.

III. Numerical Results

In this section, we present five numerical examples to validate the proposed SIM. The reference result is either from the analytical solution solved from (1) [3] or from the finite element method (FEM) simulation by the commercial software COMSOL. It is assumed that the incident plane wave is propagating along the positive $\hat{x}$ direction.

In order to quantitatively evaluate the computation accuracy of SIEs by the SIM, we define the relative error as

$$\mathrm{Err} = \frac{\left\| E_z - E_z^{\mathrm{ana}} \right\|}{\left\| E_z^{\mathrm{ana}} \right\|} \tag{19}$$

where $\|\cdot\|$ denotes the L_2 norm, and E_z and E_z^{ana} represent the electric field solved by the SIM and the analytical method, respectively. The SIM only needs to compute the zeroth-order and firstst-order special functions (Bessel functions and Hankel functions). In contrast, high-order special functions must be evaluated in the analytical solution [29], which is usually achieved by means of the recursion of n steps of nonlinear operation starting from 0th-order and 1st-order functions with n being the order of special functions. Therefore, only for the computation of special functions, the time complexity of the SIM is $O(1)$, while it is $O(n)$ for the analytical method. When the cylinder has multiple layers, the total computation cost of the SIM is $O(MN \log N)$ which has been analyzed in Section II-D. However, it is $O(nM)$ for the analytical method since the field values of all N sampling points in a single-layer interface can be solved simultaneously. For a cylinder with a large electrical size, the order n must be large enough to maintain the computation precision since the evaluation accuracy of the Bessel function is lowered for large arguments [30]. Although some optimized methods have been given previously [29] to solve high-order Bessel functions, it still has a high computation cost due to the n times iterations with nonlinear operations. Therefore, the analytical method and SIM almost have the same computational cost when the electrical size of the multilayer cylinder is small. However, the SIM outperforms the analytical method when the cylinder has a large electrical size. Another alternative method to solve the N independent matrix equations in the Fourier domain derived from (12) is using the MoM proposed in [31] for circular cylinders. When there is only one layer interface, the MoM results in diagonal matrices. The computational cost of MoM and the recursive solution by the SIM is almost the same because both of them only involve direct arithmetic operation. When the cylinder has multiple layers, the recursive solution by the SIM retains the direct arithmetic operation. However, the previous MoM needs matrix inversion because it is not easy to derive the elements of the diagonal matrix for the whole circumference of multiple layers. Consequently, the SIM outperforms MoM if the cylinder has many layers. The comparisons of analytical solutions and recursive solutions of the SIM and MoM will be shown by the second and third numerical examples in the following. All the simulations are implemented in a personal computer with an Intel(R) Core(TM) i5-8500 3.0 GHz CPU, 8.0-GB RAM memory.

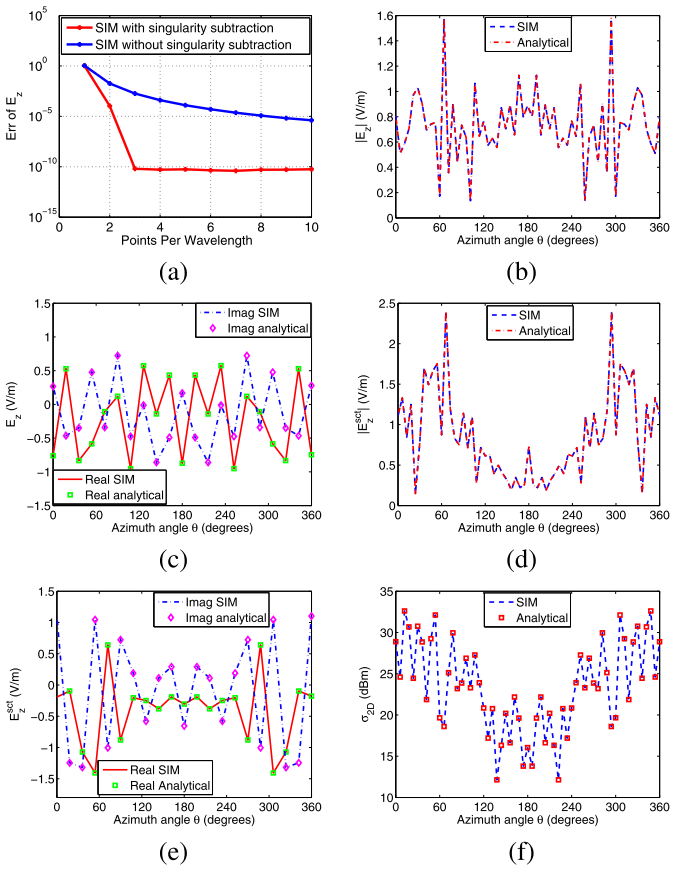

Fig. 2. EM scattering by a four-layer circular concentric magnetodielectric cylinder with the outermost radius of $500\lambda_0$ embedded in air. The fields E_z and E_z^{sct} are computed in the circumference $r_1 = 500$ m. (a) Relative errors of E_z solved by the SIM with and without the singularity subtraction. (b) Magnitude of the electric field E_z. (c) Real parts and imaginary parts of E_z. (d) Magnitude of the scattered field E_z^{sct}. (e) Real parts and imaginary parts of E_z^{sct}. (f) Bistatic RCS by the SIM and the analytical method.

A. Electrically Large Four-Layer Circular Cylinder

The large circular cylinder has four layers with the constitutive parameters (ϵ_r, μ_r) from outside to inside being (1,1), (4,2), (6,3), and (9,4). The radii from outside to inside are $r_1 = 500$ m, $r_2 = 200$ m, and $r_3 = 100$ m. The wavelength in the background medium air λ_0 is 1 m. We test the proposed method with different discretization schemes. The SD changes from 1 to 10 PPW, and the relative errors of E_z at the outermost circumference $r_1 = 500$ m are shown in Fig. 2(a). Here, the SD is calculated as the global minimum SD according to the local wavelengths. Clearly, the relative error decreases with the increase in SD. Compared with the results without singularity subtractions, the solved E_z is more precise when the singularity of Green's function is subtracted analytically. One should note that the relative error with the singularity subtraction is less than 1×10^{-10} when SD$\geqslant$3 PPW. This is the merit of the SIM [11]. Fig. 2(b) and (c) show the comparisons of the magnitude, real parts, and imaginary parts of the total field E_z in the circumference $r_1 = 500$ m when SD = 5 PPW, and the relative error is 5.5686×10^{-11}. However, the SIM only uses the zeroth and first order Hankel functions, while the order of the Hankel function in the analytical method reaches 88920 to maintain the low computation error in the

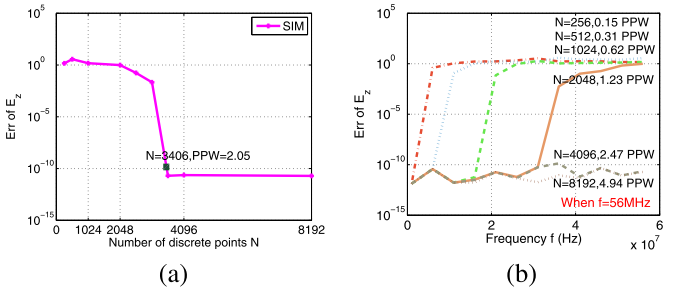

Fig. 3. Effects of sampling number N in a circumference and operating frequencies on the relative error of E_z. (a) Relative error of E_z decreases as the discrete point number N in the circumference increases. (b) Relative errors of E_z increase as the operating frequencies increase.

order of 10^{-11}. Both the real parts and imaginary parts match well between the SIM and the analytical solutions. Fig. 2(d) and (e) show the comparisons of the scattered field E_z^{sct} in the circumference $r_1 = 500$ m, and they also match well between the SIM and the analytical solutions. Fig. 2(f) shows the comparison of 2-D radar cross section (RCS) solved by the SIM and the analytical method when SD = 5 PPW and the relative error is 8.0365×10^{-11}. We can see that the RCS values match well in the whole circumference.

Fig. 3 shows the relative error of the electric field E_z obtained by the SIM when different numbers of discrete points in a circumference and different frequencies are adopted. Fig. 3(a) shows the relative error decreases with the increase in the number of discrete points N in the circumference. When $N = 3406$, SD = 2.05 PPW, and the relative error becomes less than 10^{-10}. Fig. 3(b) shows the relative error versus the operating frequency. We can see that the relative error increases when the frequency increases for a fixed SD in the circumference. However, as long as the SD is larger than 2.05 PPW, the relative error is less than 10^{-10}.

B. Electrically Small Four-Layer Circular Cylinder

In this case, we simulate a four-layer concentric cylinder which has been used for the design of conformal microstrip antennas and arrays [32], [33]. We adopt the same model size and frequency used in [33]. The most inner cylinder is PEC, and other constitutive parameters (ϵ_r, μ_r) from outside to inside are (1,1), (3.8,1), and (2.5,1). The radii from outside to inside are $r_1 = 0.053$ m, $r_2 = 0.052$ m, and $r_3 = 0.051$ m. The thickness of two middle layers is 0.001 m which is much less than the wavelength $\lambda_0 = 0.0441$ m of the incident field from the outermost layer. As shown in Fig. 4(a), the SIM shows good computational performance for the thin layers with respect to the wavelength when the singularity subtraction is adopted. Indeed, the approach with singularity subtraction has an exponential convergence so that its error decreases exponentially with the increase in the SD. Specifically, it requires only about 3 PPW to converge to an error of 5.6845×10^{-12}. In contrast, the approach without singularity subtraction requires 10 PPW to converge to an error of 3.4485×10^{-7}. The singularity subtraction technique significantly improves the convergence speed. Fig. 4(b) shows the comparison of the scattered field E_z^{sct} between the SIM results and the analytical solutions in the outermost layer

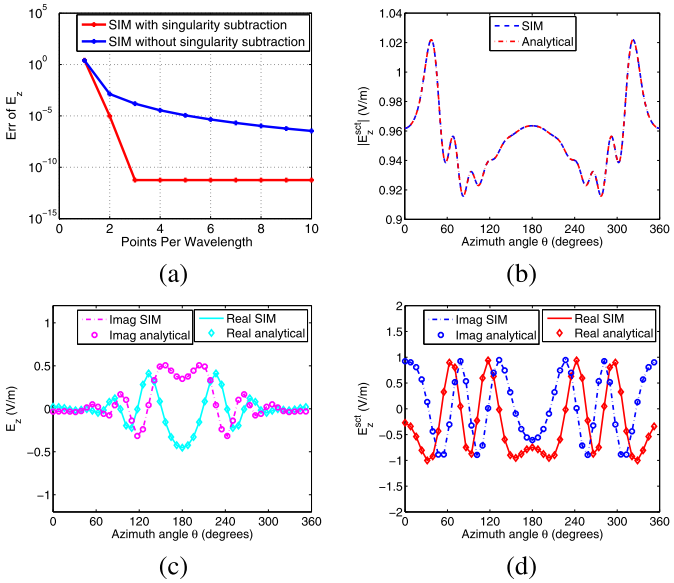

Fig. 4. EM scattering by a four-layer circular concentric magnetodielectric cylinder with the outermost radius of $1.2018\lambda_0$ embedded in air. The fields E_z and E_z^{sct} are computed in the circumference $r_1 = 0.053$ m. (a) Relative errors of E_z solved by the SIM with and without the singularity subtraction. (b) Magnitude of the scattered field E_z^{sct}. (c) Real parts and imaginary parts of E_z. (d) Real parts and imaginary parts of E_z^{sct}.

boundary r_1 when SD = 3 PPW in the background air. The relative error of E^{sct} is 1.8075×10^{-12}. Fig. 4(c) and (d) show the comparisons of the real parts and imaginary parts of the total field E_z and the scattered field E_z^{sct}. We can see that both the real parts and imaginary parts match well between the SIM and the analytical solutions. When the SD is 3 PPW, the number of discrete points on the circumference is $N = 2182$. The CPU time is 0.17188 s by the SIM and 0.18750 s by the analytic solutions. When we use MoM in the Fourier domain [31], [34], the CPU time is 0.28125 s. We can see that when the cylinder is electrically small and only has four layers, the SIM and the analytical method almost have the same computational cost. The MoM is a little slower.

C. Electrically Large 20-Layer Circular Cylinder

In this case, we increase the layer number to test the proposed method. Meanwhile, the dielectric parameters of some layers are also increased to verify the adaptability of the proposed SIM. Large permittivity and permeability values are sometimes seen in artificial EM metamaterials [35]. The circular cylinder has 20 layers. From outside to inside, the dielectric parameters (ϵ_r, μ_r) are (1,1), (3,2), (5,3), (7,4), (8,5), (9,6), (10,7), (12,8), (14,9), (16,10), (17,11), (19,12), (21,13), (23,14), (25,15), (26,16), (27,17), (28,18), (29,19), and (30,20). The radii from outside to inside are 500, 480, 450, 420, 400, 380, 350, 320, 300, 280, 250, 220, 200, 180, 160, 150, 140, 120, and 100 m. The wavelength in the background medium air λ_0 is 1 m. Therefore, this is an electrically large scatterer similar to the four-layer one in the first case. As shown in Fig. 5(a), the SIM also shows good computational performance for this 20-layer cylinder scattering when the singularity subtraction is adopted. The relative error decreases to less than 1×10^{-9} when the SD is larger than 3 PPW.

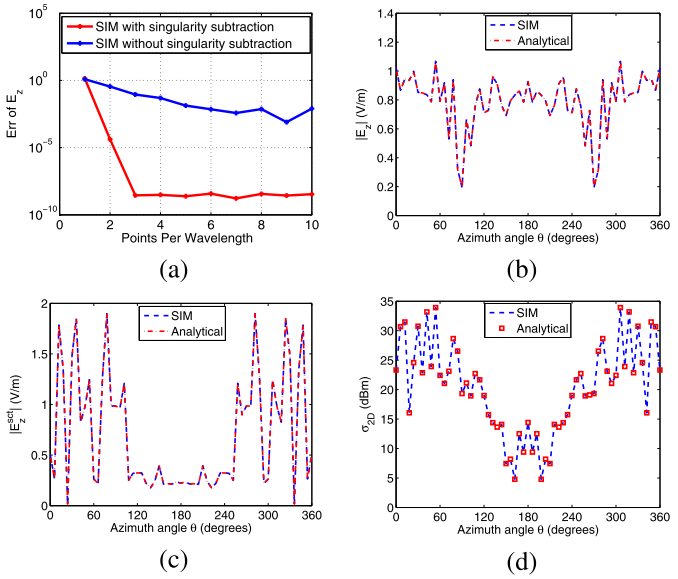

Fig. 5. EM scattering by a 20-layer circular concentric magnetodielectric cylinder with the outermost radius of $500\lambda_0$ embedded in air. The fields E_z and E_z^{sct} are computed in the circumference $r_1 = 500$ m. (a) Relative errors of E_z solved by the SIM with and without the singularity subtraction. (b) Magnitude of the electric field E_z. (c) Magnitude of the scattered field E_z^{sct}. (d) Bistatic RCS by the SIM and the analytical method.

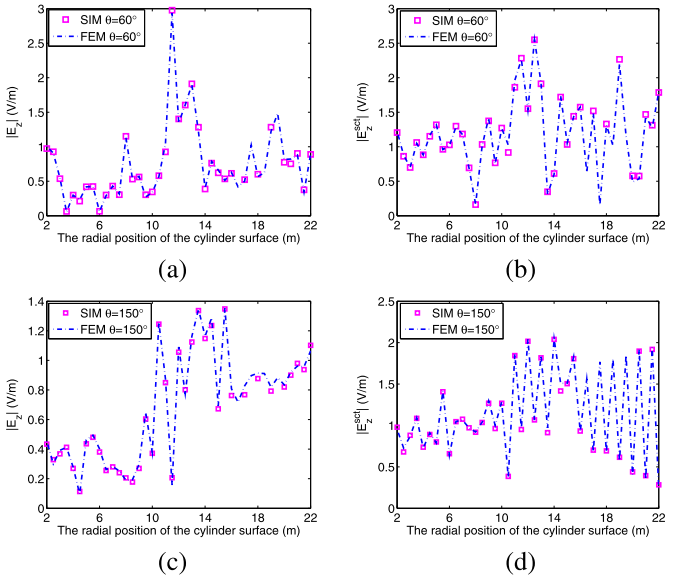

Fig. 6. EM scattering by a 20-layer circular concentric magnetodielectric cylinder with the outermost radius of $22\lambda_0$ embedded in air. Magnitudes of E_z and E^{sct} in each interface layer by two methods are compared. (a) Magnitude of E_z when the azimuth angle is 60°. (b) Magnitude of E^{sct} when the azimuth angle is 60°. (c) Magnitude of E_z when the azimuth angle is 150°. (d) Magnitude of E^{sct} when the azimuth angle is 150°.

Fig. 5(b) and (c) show the comparisons of total field E_z and the scattered field E_z^{sct} between the SIM results and the analytical solutions in the outermost layer boundary r_1 when SD = 5 PPW in the background air. The relative error of E_z is 2.4286×10^{-9} and 1.9637×10^{-9} for E^{sct}. Fig. 5(d) shows the RCS comparison, and the relative error is only 5.7018×10^{-9}. Compared with the first case, the analytical method needs the order of 240746 for the Hankel function to achieve the same accuracy while the SIM still uses the first-order Hankel function. The relative error increases around one order for the same SD. One possible reason for this difference is that the analytical solution has recursions of high-order Hankel functions between two adjacent layer boundaries, and more layers may cause extra computation errors. The CPU time is 34.9 s by the SIM, 68.3 s by the analytic solutions, and 70.8 s by MoM. Obviously, for an electrically large cylinder with 20 layers, the SIM outperforms the analytical method and MoM for the computational cost.

D. Electrically Small 20-Layer Circular Cylinder

In this case, we show the field distribution at each interface layer to verify that the method is accurate for near-field calculations. We use the FEM simulation results from COMSOL Multiphysics as the reference. In order to save the COMSOL simulation time and memory, we decrease the 20-layer concentric cylinder radii. From outside to inside, the radii are 22, 21, 20, 18, 16, 15, 14, 13, 12, 11, 10, 9, 8, 7, 6, 5, 4, 3, and 2 m. Also, the dielectric parameters (ϵ_r, μ_r) are (1,1), (1.5,0.8), (2,0.6), (2.4,0.5), (3,0.4), (1,1), (0.8,1.5), (0.6,2), (0.4,3), (0.3,4), (0.4,3), (0.6,2), (1,1), (3,0.4), (4,0.3), (3,0.4), (2,0.6), (1,1), (0.6,2), and (0.4,3). The wavelength λ_0 is also 1 m. We pick the profiles at the azimuth angle $\theta = 60°$ and 150° to compare. In order to increase the number of points to compare the radial fields, we insert one fictitious interface layer between two true interfaces, and thus, 18 interfaces are added totally. The medium parameters in both sides of the fictitious interface are the same as the original domain. Fig. 6(a) and (b) show the comparisons of the magnitude of the total fields E_z and the scattered fields E_z^{sct} at 37 points when the azimuth angle is 60° between the SIM solutions and FEM simulations. Fig. 6(c) and (d) show the comparisons of the magnitude of the total fields E_z and the scattered fields E_z^{sct} at these points when the azimuth angle is 150° between the SIM solutions and FEM simulations. We can see that the results from our SIM solutions match the FEM simulations well for all cases.

E. Five-Layer Invisibility Cloaking Cylinder

The idea of invisibility cloak was first proposed by Pendry *et al.* [36] and has become a hot topic in recent years. The ideal method is to use artificial composite materials to control or redirect the EM waves in the microwave frequency range [37], [38]. However, such metamaterials with extreme physical properties are not easy to realize in engineering. Therefore, the equivalent medium theory by replacing the inhomogeneous anisotropic materials with a more easily realized homogeneous isotropic cylindrically layered structure was developed [39], [40] and realized in laboratory experiments [41], [42].

In this case, we use the SIM to calculate the EM field surrounding a five-layer concentric cylindrical cloak. It is composed of layered isotropic magnetodielectric materials, and therefore, the SIM based on SIEs is competent for the solution. From outside to inside, the dielectric parameters (ϵ_r, μ_r) of the cloak are (1,0.09), (1,7.262), (1,0.09), (1,7.262), and (1,0.09). The wavelength λ_0 in the background medium air

TABLE I

RELATIONSHIPS AMONG THE NUMBER OF BOUNDARY LAYERS AND KEY VARIABLES, NUMBER OF EQUATION SYSTEMS, ETC., TO BE SOLVED

Number of interfaces	Number of layers	Number of indexes (p, q) for $(\mathbf{r}_p, \mathbf{r}'_q)$ at interfaces	Number of cases with $p = q$ for $(\mathbf{r}_p, \mathbf{r}'_q)$	Number of equations	Number of $L(K)$	Number of $L(K)$ with singularity	Matrix dimensions	Number of recursive equations
1	2	1	1	2×N	2×N	2×N	(2×N)×(2×N)	1×N
2	3	4	2	4×N	6×N	4×N	(4×N)×(4×N)	2×N
3	4	7	3	6×N	10×N	6×N	(6×N)×(6×N)	3×N
4	5	10	4	8×N	14×N	8×N	(8×N)×(8×N)	4×N
...	...	...	...	...	...	...	...	...
M	M+1	3M-2	M	2M×N	(4M-2)×N	2M×N	(2M×N)×(2M×N)	M×N

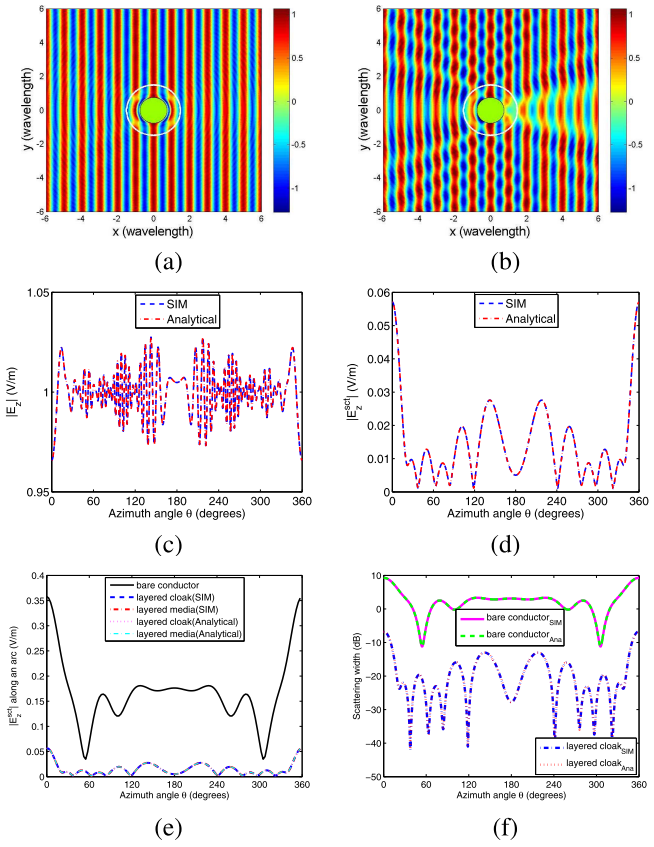

Fig. 7. EM scattering patterns for the invisibility cloak and the bare conducting cylinder. The electric field distribution when the cloak is (a) present and (b) absent. Magnitudes of (c) E_z and (d) E_z^{sct} in the circumference $r = 10.5\lambda_0$ for the layered cloak. (e) Magnitudes of the scattered field E_z^{sct} of the bare conductor, layered cloak, and layered media by the SIM and the analytical method. (f) SW of the bare conductor and layered cloak by the SIM and the analytical method evaluated for $r = 10.5\lambda_0$.

is 1 m. Because the widest range of the inner or outer radius of the cloak with a fixed medium is limited to $(2/3)\lambda_0$ to $2\lambda_0$ to ensure the invisibility performance [40], we choose the radii of 1.5, 1.0264, 1.0117, 0.8667, 0.8407, and 0.7567 m from outside to inside. Also, a conducting cylinder is enclosed at the center. Fig. 7(a) and (b) show the electric field distribution with and without the five-layer cloak. Between the black and white lines are layered cloak media, and in Fig. 7(b), they are replaced with air. It clearly demonstrates that when the layered cloak is added, EM waves still propagates in accordance with the incident waveform and direction after bypassing the cloak, and the conducting cylinder is completely invisible. Fig. 7(c) and (d) show the comparisons of the magnitudes of the total field E_z and the scattered field E_z^{sct} computed by the SIM and the analytical method in the circumference $r = 10.5$ m when SD = 3 PPW, and the relative error is 1.7786×10^{-5} and 9.4828×10^{-4}, respectively. Compared with the last two cases, the electrical size of the cylinder is smaller and the layers are less in this case, and therefore, the analytical method only needs 4192nd-order Hankel functions. Fig. 7(e) shows an intuitive comparison of three scattering phenomena involving the bare conducting cylinder, layered media without the inlaying object, and the layered cloak with the inlaying object. It is shown that when the magnetodielectric parameters of the annular cloak are properly selected, the scattering patterns of the layered cloak with and without the inlaying conductor exactly coincide, while the scattering pattern of the bare conductor has the obvious largest field magnitude. Fig. 7(f) shows the SW for the bare conductor and the layered cloak solved by the SIM and analytically, respectively. The cloak achieves an average reduction of about 10 dB for the SW in the whole circumference. We can see that the proposed the SIM based on SIEs is also capable of solving wavefield distribution for an invisibility cloak accurately.

F. Cylinder With Arbitrary Number of Layers

We generalize the magnetodielectric cylinder with arbitrary number of layers. The SIEs are formulated similar as the equation system (3). Some important parameters of the SIEs and their discretized forms are listed in Table I.

IV. CONCLUSION

We have developed the SIM for EM scattering by multilayer magnetodielectric cylinders with an arbitrary number of layers and validated its feasibility by several numerical examples including both the ordinary multilayer cylinders with different electrical sizes and the invisibility cloak cylinder. The high computation accuracy of the method with singularity subtraction is verified by the comparisons with analytical solutions and finite-element simulations. More than four orders of magnitude in accuracy improvement can be achieved with an SD less than three PPW. Instead of solving the MoM matrix iteratively, we solve the SIM final matrix equation in the Fourier domain through the convolution theorem by FFT to compute the convolution between Green's function and current source, thus saving computation time significantly. The recursive method is proposed to expedite the implementation of the

direct SIM so that its CPU complexity is only $O(MN \log N)$, and its memory complexity is only $O(MN)$. Compared with the analytical method, the proposed numerical method can achieve almost the same accuracy but avoid using the high-order Bessel and Hankel functions.

The future work will focus on two aspects. One is to extend the present method to account for multilayer dielectric cylinders with elliptical or even arbitrarily shaped cross sections. When the cross section of the cylinder is elliptical, the SIEs, Green's functions, and the recursive method mentioned in Section II are still applicable. However, after discretization, the arc length of each segment in the circumference is not the same. Therefore, nonuniform FFT must be used. When the cross section has an arbitrary shape, the boundary lines may be not smooth or irregular. The multilayer irregular surfaces can be transformed into multilayer circular smooth surfaces by using the quasi-conformal mapping technique with the mapping function expressed in terms of the solution of a Riemann-Hilbert problem which can be uniquely solved [43]. Then the SIM proposed in this article can be adopted to solve the scattering problems in the transformed domain. Another possible future work is to combine the SIM with other numerical methods such as spectral element method [44] to solve the EM scattering problem for a multilayer cylinder filled with inhomogeneous media. However, these will be left as the future work.

APPENDIX A
SUPPLEMENT TO THE RECURSION PROCESS

The relationship between adjacent electric fields for y_γ can be expressed as

$$\begin{cases} z_1(0, \mathcal{E}_{z,1}, \mathcal{E}_{z,2}) = 0 \\ y_\gamma(\mathcal{E}_{z,\gamma}, \mathcal{E}_{z,\gamma+1}) = 0, \quad 1 < \gamma < M \\ z_M(\mathcal{E}_{z,M-1}, \mathcal{E}_{z,M}, 0) = 0. \end{cases} \tag{20}$$

In order to get $\mathcal{E}_{z,\gamma}$, we recursively solve it from z_1 to y_γ (or alternatively from z_M to y_γ). From (17) we can express all known interface fields in terms of $\mathcal{E}_{z,1}$ as

$$\mathcal{E}_{z,2} = \frac{1}{c_1}(e_1 - f_1\mathcal{E}_{z,1}), \quad e_1 = d_1, \quad f_1 = b_1 \tag{21}$$

$$\mathcal{E}_{z,3} = \frac{1}{c_2}(e_2 - f_2\mathcal{E}_{z,1}), \quad e_2 = d_2 - \frac{b_2 e_1}{c_1}, \quad f_2 = a_2 - \frac{b_2 f_1}{c_1} \tag{22}$$

$$\mathcal{E}_{z,4} = \frac{1}{c_3}(e_3 - f_3\mathcal{E}_{z,1}), \quad e_3 = d_3 - \frac{a_3 e_1}{c_1} - \frac{b_3 e_2}{c_2}, \quad f_3 = -\frac{a_3 f_1}{c_1} - \frac{b_3 f_2}{c_2} \tag{23}$$

In general, for $\gamma = 3, \cdots, M-1$, we have

$$\mathcal{E}_{z,\gamma+1} = \frac{1}{c_\gamma}(e_\gamma - f_\gamma\mathcal{E}_{z,1}), \quad e_\gamma = d_\gamma - \frac{a_\gamma e_{\gamma-2}}{c_{\gamma-2}} - \frac{b_\gamma e_{\gamma-1}}{c_{\gamma-1}}, \quad f_\gamma = -\frac{a_\gamma f_{\gamma-2}}{c_{\gamma-2}} - \frac{b_\gamma f_{\gamma-1}}{c_{\gamma-1}} \tag{24}$$

Thus, for $\gamma = M-2$, from (24) we have

$$\mathcal{E}_{z,M-1} = \frac{1}{c_{M-2}}(e_{M-2} - f_{M-2}\mathcal{E}_{z,1}). \tag{25}$$

Similarly, for $\gamma = M-1$, from (24) we have

$$\mathcal{E}_{z,M} = \frac{1}{c_{M-1}}(e_{M-1} - f_{M-1}\mathcal{E}_{z,1}). \tag{26}$$

Combining (25) and (26) into (17) for $\gamma = M$ and noting $c_M = 0$, we have

$$\frac{a_M}{c_{M-2}}(e_{M-2} - f_{M-2}\mathcal{E}_{z,1}) + \frac{b_M}{c_{M-1}}(e_{M-1} - f_{M-1}\mathcal{E}_{z,1}) = d_M \tag{27}$$

which gives the solution

$$\mathcal{E}_{z,1} = \frac{\frac{a_M e_{M-2}}{c_{M-2}} + \frac{b_M e_{M-1}}{c_{M-1}} - d_M}{\frac{a_M f_{M-2}}{c_{M-2}} + \frac{b_M f_{M-1}}{c_{M-1}}} \tag{28}$$

After $\mathcal{E}_{z,1}$ is obtained by (28), $\mathcal{E}_{z,\gamma+1}$ for all $\gamma = 1, \cdots, M-1$ can be obtained from (21)–(24). The corresponding interface current densities are then obtained from (15a)–(15c). This completes the recursion.

REFERENCES

[1] K. L. Wong, Y. T. Cheng, and J. S. Row, "Resonance in a superstrate-loaded cylindrical-rectangular microstrip structure," *IEEE Trans. Microw. Theory Techn.*, vol. 41, no. 5, pp. 814–819, May 1993.

[2] H. Massoudi, C. H. Durney, P. W. Barber, and M. F. Iskander, "Electromagnetic absorption in multilayered cylindrical models of man," *IEEE Trans. Microw. Theory Techn.*, vol. MTT-27, no. 10, pp. 825–830, Oct. 1979.

[3] J. M. Jin, *Theory and Computation of Electromagnetic Fields*. Toronto, ON, Canada: Wiley, 2010.

[4] Z. Xiang and Y. Lu, "Electromagnetic dyadic Green's function in cylindrically multilayered media," *IEEE Trans. Microw. Theory Techn.*, vol. 44, no. 4, pp. 614–621, Apr. 1996.

[5] M. S. Kluskens and E. H. Newman, "Scattering by a multilayer chiral cylinder," *IEEE Trans. Antennas Propag.*, vol. 39, no. 1, pp. 91–96, Jan. 1991.

[6] M. Pastorino, M. Raffetto, and A. Randazzo, "Two-dimensional green's function for scattering and radiation problems in elliptically-layered media," *IEEE Trans. Antennas Propag.*, vol. 62, no. 4, pp. 2071–2080, Apr. 2014.

[7] H. Moon, F. L. Teixeira, and B. Donderici, "Stable pseudoanalytical computation of electromagnetic fields from arbitrarily-oriented dipoles in cylindrically stratified media," *J. Comput. Phys.*, vol. 273, pp. 118–142, Sep. 2014.

[8] Y. Leviatan and A. Boag, "Analysis of electromagnetic scattering from dielectrically coated conducting cylinders using a multifilament current model," *IEEE Trans. Antennas Propag.*, vol. 36, no. 11, pp. 1602–1607, Nov. 1988.

[9] S. Karan and V. B. Erturk, "Analysis of input impedance and mutual coupling of microstrip antennas on multilayered circular cylinders using closed-form green's function representations," *IEEE Trans. Antennas Propag.*, vol. 62, no. 11, pp. 5485–5496, Nov. 2014.

[10] J. Liu and Q. H. Liu, "A spectral integral method (SIM) for periodic and nonperiodic structures," *IEEE Microw. Wireless Compon. Lett.*, vol. 14, no. 3, pp. 97–99, Mar. 2004.

[11] Q. H. Liu, Y. Lin, J. Liu, J.-H. Lee, and E. Simsek, "A 3-D spectral integral method (SIM) for surface integral equations," *IEEE Microw. Wireless Compon. Lett.*, vol. 19, no. 2, pp. 62–64, Feb. 2009.

[12] E. Simsek, J. Liu, and Q. H. Liu, "A spectral integral method (SIM) for layered media," *IEEE Trans. Antennas Propag.*, vol. 54, no. 6, pp. 1742–11749, Jun. 2006.

[13] Y.-K. Li, J. Hu, W.-F. Huang, Z.-P. Nie, and Q. H. Liu, "A spectral integral method for smooth multilayered bodies of revolution," *IEEE Trans. Antennas Propag.*, vol. 65, no. 8, pp. 4146–4154, Aug. 2017.

[14] A. V. Boriskin and A. I. Nosich, "Whispering-gallery and Luneburg-lens effects in a beam-fed circularly layered dielectric cylinder," *IEEE Trans. Antennas Propag.*, vol. 50, no. 9, pp. 1245–1249, Sep. 2002.

[15] R. S. Zaridze, R. Jobava, G. Bit-Banik, D. Karkasbadze, D. P. Economou, and N. K. Uzunoglu, "The method of auxiliary sources and scattered field singularities (caustics)," *J. Electromagn. Waves Appl.*, vol. 12, no. 11, pp. 1491–1507, Jan. 1998.

[16] N. L. Tsitsas, E. G. Alivizatos, D. I. Kaklamani, and H. T. Anastassiu, "Optimization of the method of auxiliary sources (MAS) for oblique incidence scattering by an infinite dielectric cylinder," *Elect. Eng.*, vol. 89, no. 5, pp. 353–361, May 2007.
[17] J. Helsing and A. Karlsson, "An accurate boundary value problem solver applied to scattering from cylinders with corners," *IEEE Trans. Antennas Propag.*, vol. 61, no. 7, pp. 3693–3700, Jul. 2013.
[18] C. Zhu, L. Liu, Z. Song, Y. Liu, and Q. H. Liu, "An efficient exact numerical solution for scattering by a circular cylinder," *IEEJ Trans. Elect. Electron. Eng.*, vol. 11, pp. S3–S10, Dec. 2016.
[19] R. Leis, "Über das neumannsche randwertproblem für die helmholtzsche schwingungsgleichung," *Arch. Rat. Mech. Anal.*, vol. 2, pp. 101–113, Jan. 1958.
[20] A. J. Burton and G. F. Miller, "The application of integral equation methods to the numerical solution of some exterior boundary-value problems," *Proc. Roy. Soc. London A, Math. Phys. Sci.*, vol. 323, pp. 201–210, Jun. 1971.
[21] S. Rao, D. Wilton, and A. Glisson, "Electromagnetic scattering by surfaces of arbitrary shape," *IEEE Trans. Antennas Propag.*, vol. AP-30, no. 3, pp. 409–418, May 1982.
[22] W. C. Chew, *Waves and Fields in Inhomogeneous Media* New York, NY, USA: IEEE Press, 1995.
[23] F. Q. Hu, "A fast numerical solution of scattering by a cylinder: Spectral method for the boundary integral equations," *J. Acoust. Soc. Amer.*, vol. 96, no. 6, pp. 3693–3703, Dec. 1994.
[24] F. Q. Hu, "A spectral boundary integral equation method for the 2D Helmholtz equation," *J. Comput. Phys.*, vol. 120, no. 2, pp. 340–347, Sep. 1995.
[25] S. I. Zaman, "A comprehensive review of boundary integral formulations of acoustic scattering problems," *Sultan Qaboos Univ. J. Sci.*, vol. 5, p. 281, May 2017.
[26] G. T. Schuster, "A fast exact numerical solution for the acoustic response of concentric cylinders with penetrable interfaces," *J. Acoust. Soc. Amer.*, vol. 87, no. 2, pp. 495–502, Feb. 1990.
[27] J.-S. Lee, T.-L. Song, J.-K. Du, and J.-G. Yook, "Near-field to far-field transformation based on stratton-chu fomula for EMC measurements," in *Proc. IEEE Antennas Propag. Soc. Int. Symp.*, Jul. 2013, pp. 606–607.
[28] W.-F. Huang, Y. Ren, and Q. H. Liu, "Solid-angle error in the magnetic-field integral equation for perfectly electric conducting objects," *IEEE Trans. Antennas Propag.*, vol. 64, no. 3, pp. 1158–1163, Mar. 2016.
[29] S. Zhang and J. M. Jin, *Computation of Special Functions*. New York, NY, USA: Wiley, 1996.
[30] C. F. du Toit, "The numerical computation of Bessel functions of the first and second kind for integer orders and complex arguments," *IEEE Trans. Antennas Propag.*, vol. 38, no. 9, pp. 1341–1349, Sep. 1990.
[31] G. C. Hsiao and R. E. Kleinman, "Mathematical foundations for error estimation in numerical solutions of integral equations in electromagnetics," *IEEE Trans. Antennas Propag.*, vol. 45, no. 3, pp. 316–328, Mar. 1997.
[32] J. Sun, C.-F. Wang, L.-W. Li, and M.-S. Leong, "Further improvement for fast computation of mixed potential Green's functions for cylindrically stratified media," *IEEE Trans. Antennas Propag.*, vol. 52, no. 11, pp. 3026–3036, Nov. 2004.
[33] J. Sun, C. F. Wang, L. W. Li, and M. S. Leong, "Closed form Green's functions for ρ-oriented electrical source in cylindrically stratified media," in *Proc. IEEE Antennas Propag. Soc. Int. Symp.*, vol. 2, Jun. 2003, pp. 804–807.
[34] K. F. Warnick and W. C. Chew, "Numerical simulation methods for rough surface scattering," *IEEE Trans. Antennas Propag.*, vol. 11, no. 1, pp. R1–R30, 2001.
[35] H. Oraizi and A. Abdolali, "Design and optimization of planar multilayer antireflection metamaterial coatings at ku band under circularly polarized oblique plane wave incidence," *Prog. Electromagn.*, vol. 3, pp. 1–18, 2008.
[36] J. B. Pendry, "Controlling electromagnetic fields," *Science*, vol. 312, no. 5781, pp. 1780–1782, Jun. 2006.
[37] S. A. Cummer, B.-I. Popa, D. Schurig, D. R. Smith, and J. Pendry, "Full-wave simulations of electromagnetic cloaking structures," *Phys. Rev. E, Stat. Phys. Plasmas Fluids Relat. Interdiscip. Top.*, vol. 74, no. 3, Sep. 2006, Art. no. 036621.
[38] F. Zolla, S. Guenneau, A. Nicolet, and J. B. Pendry, "Electromagnetic analysis of cylindrical invisibility cloaks and the mirage effect," *Opt. Lett.*, vol. 32, no. 9, pp. 1069–1071, May 2007.
[39] Y. Huang, Y. Feng, and T. Jiang, "Electromagnetic cloaking by layered structure of homogeneous isotropic materials," *Opt. Express*, vol. 15, no. 18, pp. 11133–11141, Sep. 2007.
[40] Z. Yu, Y. Feng, X. Xu, J. Zhao, and T. Jiang, "Optimized cylindrical invisibility cloak with minimum layers of non-magnetic isotropic materials," *J. Phys. D: Appl. Phys.*, vol. 44, no. 18, May 2011, Art. no. 185102.
[41] Z. Ruan, M. Yan, C. W. Neff, and M. Qiu, "Confirmation of cylindrical perfect invisibility cloak using Fourier–Bessel analysis," *Phys. Rev. Lett.*, vol. 99, no. 113903, pp. 1–10, 2007.
[42] W. X. Jiang, T. J. Cui, X. M. Yang, Q. Cheng, R. Liu, and D. R. Smith, "Invisibility cloak without singularity," *Appl. Phys. Lett.*, vol. 93, no. 19, Nov. 2008, Art. no. 194102.
[43] M. M. S. Nasser, "A boundary integral equation for conformal mapping of bounded multiply connected regions," *Comput. Methods Funct. Theory*, vol. 9, no. 1, pp. 127–143, Apr. 2009.
[44] J. Niu, M. Luo, Y. Fang, and Q. H. Liu, "Boundary integral spectral element method analyses of extreme ultraviolet multilayer defects," *J. Opt. Soc. Amer. A, Opt. Image Sci.*, vol. 31, no. 10, pp. 2203–2209, Oct. 2014.

Zhen Guan received the B.S. degree in mathematics and applied mathematics and the M.S. degree in pure mathematics from the Tianjin University of Technology and Education, Tianjin, China, in 2014 and 2017, respectively. She is currently pursuing the Ph.D. degree in computational science at Xiamen University, Xiamen, China.

Her research interests include the fast algorithms for computational electromagnetics and electromagnetic scattering and inverse scattering problems.

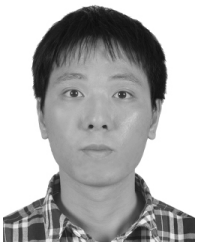

Yuxian Zhang (Member, IEEE) received the B.S. and M.S. degrees from the Tianjin University of Technology and Education, Tianjin, China, in 2012 and 2015, respectively. He received the Ph.D. degree from the Institute of Electromagnetics and Acoustics, Xiamen University, Xiamen, China, in 2019.

He is currently an Associate Professor at the Institute of Microscale Optoelectronics, Shenzhen University, Shenzhen, China. His current research interests include subsurface reverse-time migration imaging and computational electromagnetics.

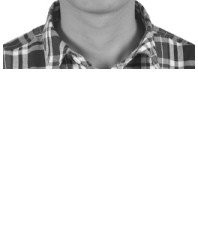

Feng Han (Member, IEEE) received the B.S. degree in electronic science from Beijing Normal University, Beijing, China, in 2003, the M.S. degree in geophysics from Peking University, Beijing, in 2006, and the Ph.D. degree in electrical engineering from Duke University, Durham, NC, USA, in 2011.

He is currently an Assistant Professor with the Institute of Electromagnetics and Acoustics, Xiamen University, Xiamen, China. His research interests include ionosphere remote sensing by radio atmospherics, electromagnetic full-wave inversion by integral equations, reverse time migration image, and the design of an electromagnetic detection system.

Chunhui Zhu was born in Harbin, Heilongjiang, China, in 1985. She received the B.S. degree in information and computational science from Jilin University, Changchun, China, in 2007 , and the Ph.D. degree in control science and engineering from the Harbin Institute of Technology, Harbin, China, in 2012.

From 2009 to 2011, she was a cocultured Ph.D. student with the Department of Electrical Engineering, Duke University, Durham, NC, USA. Since 2013, she has been an Assistant Professor with the Institute of Electromagnetics and Acoustics, Xiamen University, Xiamen, China. Her current research interest includes fast algorithms for computational electromagnetics and their applications in engineering.

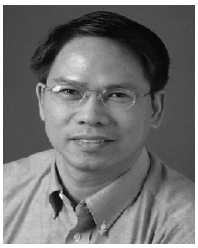

Qing Huo Liu (Fellow, IEEE) received the B.S. and M.S. degrees in physics from Xiamen University, Xiamen, China, and the Ph.D. degree in electrical engineering from the University of Illinois at Urbana–Champaign, Champaign, IL, USA.

From September 1986 to December 1988, he was a Research Assistant with the Electromagnetics Laboratory, University of Illinois at Urbana–Champaign, where he was a Post-Doctoral Research Associate from January 1989 to February 1990. He was a Research Scientist and the Program Leader with Schlumberger-Doll Research, Ridgefield, CT, USA, from 1990 to 1995. From 1996 to May 1999, he was an Associate Professor with New Mexico State University, Las Cruces, NM, USA. Since June 1999, he has been with Duke University, Durham, NC, USA, where he is currently a Professor of electrical and computer engineering. He has also been the Founder and Chairman of Wave Computation Technologies, Inc., since 2005. His research interests include computational electromagnetics and acoustics, inverse problems, and their application in nanophotonics, geophysics, biomedical imaging, and electronic packaging. He has published widely in these areas.

Dr. Liu is a Fellow of the Acoustical Society of America, Electromagnetics Academy, and the Optical Society of America. He received the 1996 Presidential Early Career Award for Scientists and Engineers (PECASE) from the White House, the 1996 Early Career Research Award from the Environmental Protection Agency, the 1997 CAREER Award from the National Science Foundation, the 2017 Technical Achievement Award, the 2018 Computational Electromagnetics Award from the Applied Computational Electromagnetics Society, the 2018 Harrington-Mittra Award in Computational Electromagnetics from the IEEE Antennas and Propagation Society, and the ECE Distinguished Alumni Award from the University of Illinois at Urbana–Champaign in 2018. He has served as an IEEE Antennas and Propagation Society Distinguished Lecturer, and as the Founding Editor-in-Chief for the IEEE JOURNAL ON MULTISCALE AND MULTIPHYSICS COMPUTATIONAL TECHNIQUES.